Article

Simulations of Stochastic Sensing of Proteins

Chung Yin Kong, and M. Muthukumar

J. Am. Chem. Soc., **2005**, 127 (51), 18252-18261• DOI: 10.1021/ja055695o • Publication Date (Web): 02 December 2005

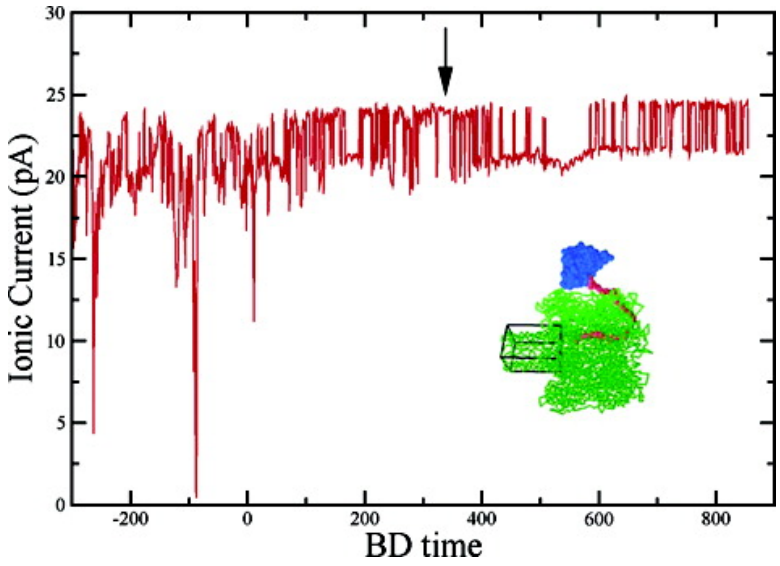

More About This Article

Additional resources and features associated with this article are available within the HTML version:

- Supporting Information
- Links to the 4 articles that cite this article, as of the time of this article download
- Access to high resolution figures
- Links to articles and content related to this article
- Copyright permission to reproduce figures and/or text from this article

View the Full Text HTML

J|A|C|S
ARTICLES
Published on Web 12/02/2005

Simulations of Stochastic Sensing of Proteins

Chung Yin Kong and M. Muthukumar*

Contribution from the Department of Polymer Science and Engineering, University of Massachusetts at Amherst, Amherst, Massachusetts 01003

Received August 19, 2005; E-mail: muthu@polysci.umass.edu

Abstract: We have performed Langevin dynamics and Poisson−Nernst−Planck calculations to simulate detection of proteins by genetically engineered α-hemolysin channels. In the recent stochastic sensing experiments, one end of a flexible polymer chain is permanently anchored inside the protein channel at a specified location, and the other end undergoes complexation with an analyte. Our simulations, using coarse-grained modeling, reproduce all essential qualitative results of the electrophysiology measurements of stochastic sensing. In addition, the underlying macromolecular mechanisms behind stochastic sensing are revealed in vivid details. The entropic fluctuations of the conformations of the tethered polymer chain dictate crucially the unique signatures of the ionic current trace of the channel and provide design rules for successful stochastic sensing. The origin of strong fluctuations in the ionic current of the channel is found to arise from the obstruction of the entrance at the β-barrel of the channel by the fluctuating segments of the tether. Silencing of the pore is due to the suppression of conformational fluctuations of the chain, and the permanent blockade of ionic current is due to the threading of the tether through the channel. The onset of silencing and permanent blockade of the channel current cannot necessarily be attributed to the capture of analytes. In order for detection events to be timed accurately, the length and anchoring location of the tether must be tuned appropriately.

1. Introduction

Selective sensing of macromolecules and small ions by protein channels is the foundation of signal transduction in many biological processes. While an understanding of macromolecular aspects of these processes continues to be sought, there have recently been experimental demonstrations[1−9] of sensing the chemical identity of single analyte molecules, using ionic currents through genetically engineered protein channels. This new technique, called stochastic sensing, is motivated by the demands in the context of pharmaceutical screening and biological warfare agents. The early experimental investigations in the development of stochastic sensors, to detect single molecules such as DNA/RNA and proteins, have provided very exciting results and many puzzles. In this paper, we focus on one of these experimental situations, that is, stochastic sensing of proteins by genetically modified synthetic protein channels using ionic current measurements.[6] We address, using simultaneous Langevin dynamics simulations of polymer conformations and computation of ionic currents through protein channels, macromolecular mechanisms behind the stochastic sensing technique.

In the basic setup[10−15] of these single-molecule sensing experiments, a protein channel is first assembled in a phospholipid bilayer separating a donor chamber (called *cis*) and a recipient chamber (called *trans*), with both chambers filled with a buffer and an added salt. The protein pore is a heptameric self-assembly of α-hemolysin (αHL) with a mushroom shape, consisting of a vestibule on the *cis* side and a transmembrane β-barrel toward the *trans* side. The length of the channel is about 10 nm. When an external voltage is applied across the membrane, the channel allows passage of small ions, and the resulting ionic current is measured. When this experiment is repeated with single-stranded DNA/RNA originally present in the *cis* chamber and the positive electrode on the *trans* side, the measured ionic current decreases significantly whenever the polynucleotide passes through the channel. The frequency of occurrence of blockade events reveals the analyte concentration, whereas the current signature (duration and amplitude of blocked current) reveals the identity of the analyte.

(1) Braha, O.; Walker, B.; Cheley, S.; Kasianowicz, J. J.; Song, L. Z.; Gouaux, J. E.; Bayley, H. *Chem. Biol.* **1997**, *4*, 497.
(2) Gu, L. Q.; Braha, O.; Conlan, S.; Cheley, S.; Bayley, H. *Nature* **1999**, *398*, 686.
(3) Sanchez-Quesada, J.; Ghadiri, M. R.; Bayley, H.; Braha, O. *J. Am. Chem. Soc.* **2000**, *122*, 11757.
(4) Braha, O.; Gu, L. Q.; Zhou, L.; Lu, X. F.; Cheley, S.; Bayley, H. *Nat. Biotechnol.* **2000**, *18*, 1005.
(5) Howorka, S.; Movileanu, L.; Lu, X. F.; Magnon, M.; Cheley, S.; Braha, O.; Bayley, H. *J. Am. Chem. Soc.* **2000**, *122*, 2411.
(6) Movileanu, L.; Howorka, S.; Braha, O.; Bayley, H. *Nat. Biotechnol.* **2000**, *18*, 1091.
(7) Movileanu, L.; Bayley, H. *Proc. Natl. Acad. Sci. U.S.A.* **2001**, *98*, 10137.
(8) Bayley, H.; Cremer, P. S. *Nature* **2001**, *413*, 226.
(9) Cheley, S.; Gu, L. Q.; Bayley, H. *Chem. Biol.* **2002**, *9*, 829.
(10) Kasianowicz, J. J.; Brandin, E.; Branton, D.; Deamer, D. W. *Proc. Natl. Acad. Sci. U.S.A.* **1996**, *93*, 13770−13773.
(11) Bezrukov, S. M.; Vodyanoy, I.; Brutyan, R. A.; Kasianowicz, J. J. *Macromolecules* **1996**, *29*, 8517−8522.
(12) Akeson, M.; Branton, D.; Kasianowicz, J. J.; Brandin, E.; Deamber, D. W. *Biophys. J.* **1999**, *77*, 3227−3233.
(13) Henrickson, S. E.; Misakian, M.; Robertson, B.; Kasianowicz, J. J. *Phys. Rev. Lett.* **2000**, *85*, 3057−3060.
(14) Meller, A.; Nivon, L.; Brandin, E.; Golovchenko, J.; Branton, D. *Proc. Natl. Acad. Sci. U.S.A.* **2000**, *97*, 1079−1084.
(15) Meller, A.; Nivon, L.; Branton, D. *Phys. Rev. Lett.* **2001**, *86*, 3435−3438.

10.1021/ja055695o CCC: $30.25

The extent, duration, and frequency of channel current blockades depend sensitively on the chemical nature of molecules translocating through the channel and form the basis of stochastic sensing. We have recently modeled[16] successfully the ionic traces for the passage of polynucleotides through the αHL channel. In the present paper, we extend our modeling technique to the situation of sensing single molecules by complexation with a complementary molecule, which in turn is borne by the channel by suitable modifications. In this adaptation[6] of stochastic sensing, one end of poly(ethylene glycol) (PEG) is covalently attached to a desired site in the lumen of the vestibule of the αHL pore by genetic engineering, and the other end of PEG carries a ligand for the target analyte.

The operational principle of this strategy has been demonstrated[6] by using streptavidin as the analyte and biotin as the ligand attached to the free end of PEG. The other end of the PEG is anchored at position 106, as an example, within the central cavity of αHL. The PEG molecule fluctuates in conformations and, consequently, modifies the flow of small ions through the channel. Unlike the unmodified pore, the ionic current exhibits many negative short-lived and high amplitude blockades, reflecting fluctuations of conformations of the PEG tether. Whenever complexation occurs between the analyte molecule and the ligand attached to PEG, the ionic current trace is expected to exhibit a unique signature. Indeed, it was found[6] that the ionic current through the pore suddenly became silent, and this was taken as an indicator of complexation. In contrast, if the analyte was dispersed in the *trans* chamber, it was experimentally found[6] that the pore current was blocked completely when complexation occurred. The goal of the present paper is to obtain molecular details behind these observations, by using molecular modeling.

One of the key issues in the design of the sensor is the probability of finding the reactive end of the PEG tether to complex with the analyte, as a function of the location of the anchor inside the vestibule, tether length, and the extent of excluded volume interactions for PEG in the ionic solution. Although there are many theoretical descriptions of tethered polymer chains in simple geometries, such as spherical,[17−19] cylindrical,[20,21] and planar,[22−24] there are no analytical calculations for the geometry of αHL. In view of this, we have performed Langevin dynamics simulations of the tether and report quantitative details for the probability distribution for the location of the tether end arising from entropic and excluded volume forces due to confinement inside the vestibule. We have also monitored the complexation reaction between the tether end and an analyte dispersed in either the *cis* or *trans* chamber. The other key issue in the sensing process is the relation between the ionic current trace and the underlying molecular processes. We have investigated this relation by computing the ionic current using the Poisson−Nernst−Planck (PNP) formalism in conjunction with the Langevin dynamics simulation of complexation process.

A brief summary of the major results of modeling presented here is the following. The PNP formalism provides a good description of measured ionic current through the αHL pore when the pore is unmodified and when the pore contains the PEG tether. The sharp and brief blockades observed in experiments are due to fluctuations in chain conformations of PEG and, in particular, due to the eclipsing of the mouth of the β-barrel by PEG segments inside the vestibule. The silencing of the pore is due to stretching of the tether after complexation, and not necessarily at the instant of complexation. However, an appropriate choice of the tether length can be chosen to synchronize the complexation event and silencing of the pore. In contrast, binding in *trans* chamber always leads to permanent blockade of pore current. To use the strategy of fishing-line for sensing analytes, our simulations can be used to design the length of the tether and its anchoring location.

2. Simulation Method

The protein pore, *Staphylococcus aureus* α-hemolysin,[25] is represented by a united atom model, and the residues of the pore are made up of beads of the same size.[16] The coordinates of the residues are extracted from the Protein Data Bank (PDB). It has been demonstrated that this pore can remain open for periods of the order of tens of seconds in concentrated salt solutions.[26] In view of this observation, the protein pore is not allowed to move. In addition, the ionic current through α-HL (in the absence of any polymer) is found experimentally to be stable once the channel is open. In general, the current through a channel depends on tiny details of the locations of permanent charges. Thus the finding of a stable current implies that the locations of permanent charges are stable on the time scale of measurements. In view of this, we have used a static model of the channel protein in the present study. The poly(ethylene glycol) (PEG) molecule is also represented by the united atom model, and an electrically neutral bead represents two repeat units of PEG. In the calculations, one simulation unit of length is 6.6 Å. The potential interaction between nonbonded beads of the chain is taken as the Lennard-Jones (LJ) potential

$$U_{\mathrm{LJ}} = \epsilon_{\mathrm{LJ}}\left[\left(\frac{\sigma}{r}\right)^{12} - 2\left(\frac{\sigma}{r}\right)^{6}\right] \tag{2.1}$$

where ϵ_{LJ} is the interaction strength, $\sigma = 0.4$ is the location of the potential minimum, and r is the distance between two beads. ϵ_{LJ} is used as the unit of energy. The potential energy associated with bond-stretching of each bond of the chain is taken to be

$$U_{\mathrm{bond}} = k(l - l_0)^2 \tag{2.2}$$

where l is the bond length and the equilibrium bond length $l_0 = 0.5$ in simulation length unit. The spring constant k is 2×10^4 in simulation units of energy per length squared.

The polymer is tethered at different positions on the pore. Although there have been experiments suggesting that the interaction between PEG and the pore may be attractive,[11] the exact interaction between PEG and the pore is still not known. Here we focus on the complex geometry of the pore and model the polymer−pore interaction by a hardcore repulsive potential. The hardcore distance between the polymer bead and protein is 0.7 in simulation length units. A cartoon representation and a simulation snapshot of the system are shown in Figure 1. Streptavidin is a tetrameric protein which is able to bind up to four

(16) Kong, C.; Muthukumar, M. *Electrophoresis* **2002**, *23*, 2697.
(17) Muthukumar, M. *Phys. Rev. Lett.* **2001**, *86*, 3188.
(18) Muthukumar, M. *J. Chem. Phys.* **2003**, *118*, 5174.
(19) Kong, C. Y.; Muthukumar, M. *J. Chem. Phys.* **2004**, *120*, 3460.
(20) (a) Daoud, M.; Degennes, P. G. *J. Physique* **1977**, *38*, 85. (b) Sotta, P.; Lesne, A.; Victor, J. M. *J. Chem. Phys.* **2000**, *113*, 6966.
(21) Hermsen, G. F.; de Geeter, B. A.; van der Vegt, N. F. A.; Wessling, M. *Macromolecules* **2002**, *35*, 5267.
(22) Subramanian, G.; Williams, D. R. M.; Pincus, P. A. *Europhys. Lett.* **1995**, *29*, 285.
(23) Milchev, A.; Yamakov, V.; Binder, K. *Europhys. Lett.* **1999**, *47*, 675.
(24) Cifra, P.; Bleha, T. *Macromolecules* **2001**, *34*, 605.
(25) Song, L. Z.; Hobaugh, M. R.; Shustak, C.; Cheley, S.; Bayley, H.; Gouaux, J. E. *Science* **1996**, *274*, 1859.
(26) Korchev, Y. E.; Bashford, C. L.; Alder, G. M.; Kasianowicz, J. J.; Pasternak, C. A. *J. Membr. Biol.* **1995**, *147*, 233−239.

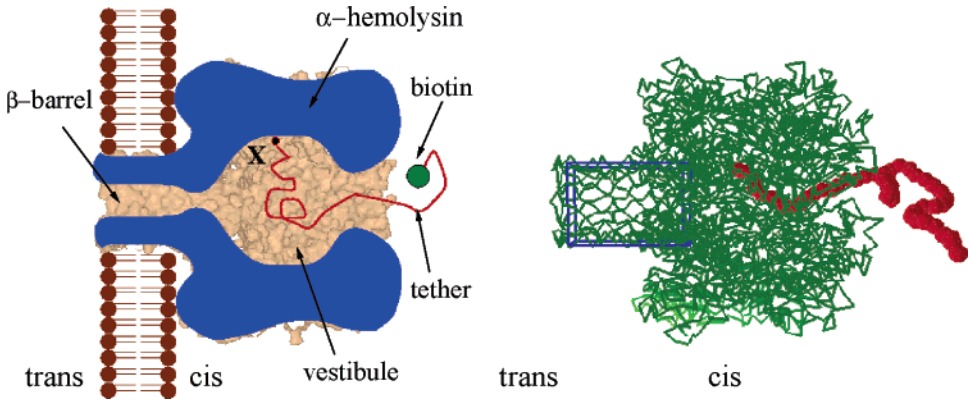

Figure 1. An illustration of a polymer tethered inside α-hemolysin. The left picture is a cartoon representation of the system. The right picture is a snapshot taken from the simulation.

biotin molecules.[27] The streptavidin is modeled by a collapsed flexible polymer with 450 beads of same size. The potential interaction between nonbonded beads of the model streptavidin is again modeled by the LJ potential with $\epsilon_{LJ} = 50$ and $\sigma = 0.5$ in their dimensionless units mentioned above. The model streptavidin is too large to fit into the α-hemolysin. At pH 7.0 (the condition of the stochastic sensing experiments), streptavidin has been reported to have a net negative surface charge.[27] To account for this fact, our model streptavidin has one negative charge on each polymer bead. The net charge is taken to be so high to make the complexation process faster in the simulation. The biotin molecule is represented by one extra neutral bead at the end of the PEG chain. The specific interaction energy between the wild-type streptavidin and a biotin molecule is 30 k_BT, and a mutant streptavidin has a considerably lower binding affinity for biotin, ~16 k_BT.[28−30] We model the interaction potential between the biotin and streptavidin by the LJ potential. The value of σ is 0.45 for biotin−streptavidin, and the values of ϵ_{LJ} are 30 and 16 for wild-type streptavidin and a mutant streptavidin, respectively. The interaction between the polymer beads (except for the biotin end) and the beads of streptavidin is taken to be the same as the intrachain interaction. To speed up the capture simulations, the biotin is allowed to bind to any site on the streptavidin's surface. It is to be noted that the present crude model of biotin and streptavidin is designed to focus on the main issues of stochastic sensing and to allow extensive low cost computation. Further work on this system and on other binding systems would benefit from models in atomic detail.

In our simulations, the membrane which separates the *cis* and *trans* chambers is modeled by a hard wall. The pore is embedded into the wall, with the vestibule of the pore submerged in the *cis* chamber. The central axis of the protein pore is aligned with the *X*-axis of the system, and the end of the β-barrel (narrow channel of the pore) is placed at $X = 0$. With the exception of the anchoring bead, the polymer chain is allowed to move by integrating the equations of motion according to the methodology of Langevin dynamics (LD).[31]

In the Langevin dynamics simulations used here for the time evolution of polymer conformations, the dynamics of the *i*th bead is taken as

$$m\frac{d^2\mathbf{r}_i}{dt^2} = -\zeta\mathbf{v}_i - \nabla_{\mathbf{r}i}U + \mathbf{F}_i(t) \tag{2.3}$$

where $\mathbf{r}_i$, m, and ζ are the position vector, mass, and the friction coefficient, respectively, of the *i*th bead. $\mathbf{F}_i(t)$ is the random force from the solvent bath acting on the *i*th bead and is constructed to satisfy the fluctuation−dissipation theorem

$$\langle \mathbf{F}_i(t)\cdot\mathbf{F}_j(t')\rangle = \delta_{ij}6k_BT\zeta\delta(t-t') \tag{2.4}$$

where t is the time and δ is the usual delta function. U in eq 2.3 is the total potential energy of the *i*th bead and consists of two contributions

$$U = U_{bond} + U_{LJ} \tag{2.5}$$

as given above. U_{LJ} arises from three sources, that is, intrachain, polymer−αHL, and polymer−streptavidin, as detailed above. The velocity−Verlet finite-differencing scheme[31] has been used for integration of eq 2.3. The mass and friction coefficient are taken to be unity for all beads of the chain. The time variable in the simulations is in units of the dimensionless time $t_0 = \sqrt{m\sigma^2/\epsilon_{LJ}}$. Due to the nature of the present coarse-graining without an explicit description of solvent molecules (and hydrodynamics), it is impossible to associate real time with t, unlike molecular dynamics simulations.[32] A crude estimate of t_0 is about 0.15 μs, for the present set of values of various parameters. Therefore, one BD time corresponds roughly to 0.15 μs in the results given below.

The small free ions in water are treated as a continuous medium with charge density, $C_i(\mathbf{r},t)$, at location $\mathbf{r}$ and time t of the *i*th ion species (counterions of the pore, and small ions from the added salt). The ionic current and local electrostatic potential are calculated by using the three-dimensional Poisson−Nernst−Planck (PNP) equations.[33−35]

The equation for the time-evolution of $C_i(\mathbf{r},\mathbf{t})$ is given by

$$\frac{\partial C_i(\mathbf{r},t)}{\partial t} = -\nabla\cdot\mathbf{J}_i \tag{2.6}$$

where the flux $\mathbf{J}_i$ is given by the sum of diffusive and drift parts

$$\mathbf{J}_i = -D_i\left(\nabla C_i(\mathbf{r},t) + \frac{Z_iC_i}{k_BT}\nabla V\right) \tag{2.7}$$

Here, Z_i and D_i are, respectively, the charge and diffusion coefficient of the *i*th species (except the polymer) contributing to the ionic current. k_BT is the Boltzmann constant times the absolute temperature.

The electrostatic potential, V, is given by the Poisson equation

$$\epsilon_0\nabla\cdot[\epsilon(\mathbf{r})\nabla V(\mathbf{r})] = -\rho_{ex} - \sum_i Z_iC_i(\mathbf{r}) \tag{2.8}$$

where ϵ_0 is the permittivity of the vacuum and $\epsilon(\mathbf{r})$ is the inhomoge-

(27) Chaiet, L.; Wolf, F. *J. Arch. Biochem. Biophys.* **1964**, *106*, 1−5.
(28) Green, N. M. *Adv. Protein Chem.* **1975**, *29*, 85−133.
(29) Miyamoto, S.; Kollman, P. A. *Proteins* **1993**, *16*, 226.
(30) Chilkoti, A.; Tan, P. H.; Stayton, P. S. *Proc. Natl. Acad. Sci. U.S.A.* **1995**, *92*, 1754.
(31) Allen, M. P.; Tildesley, D. J. *Computer Simulation of Liquids*; Oxford: New York, 1987.
(32) Aksimentiev, A.; Schulten, K. *Biophys. J.* **2005**, *88*, 3745.
(33) Eisenberg, R. S. *J. Membr. Biol.* **1996**, *150*, 1.
(34) Kurnikova, M. G.; Coalson, R. D.; Graf, P.; Nitzan, A. *Biophys. J.* **1999**, *76*, 642.
(35) Corry, B.; Kuyucak, S.; Chung S. H. *Biophys. J.* **2000**, *78*, 2364.

neous dielectric constant. The values of $\epsilon(\mathbf{r})$ were set to 80 for water and 2 for the membrane, and the beads constituting the proteins and PEG. ρ_{ex} is the charge density for all fixed charges in the system, such as the charges on the proteins. The external applied voltage is imposed by fixing the potential at the boundaries. In all of our calculations, the solution contains 0.3 M KCl. The values of D_i are 1.96×10^{-5} cm^2 s^{-1} for K^+ ions and 2.03×10^{-5} cm^2 s^{-1} for Cl^- ions. The magnitude of the applied voltage is 100 mV.

We have numerically solved the above eqs 2.6−2.8 in the steady-state limit. In general, the numerical solution of these equations is delicate in terms of the resolution of the discretized space and integration step. The interested reader should consult refs 36 and 37 for rich details. In the present work, we have solved these equations by the successive over-relaxation method with a grid spacing of 1 Å, by following ref 34. First we start with $V(X)$ due to the externally applied electrostatic potential gradient across a membrane of dielectric constant 2 without any pore. The concentrations of the cations and anions (C_+ and C_-, respectively) of the dissolved electrolyte on both sides of the membrane are uniform. Under these conditions, the potential V is simply a ramp. Then, the coordinates of beads of the pore are read in. Next, using the successive over-relaxation method, V, C_+, and C_- are computed iteratively until they converge within the tolerance levels of $\Delta V = 10^{-8}$ V, and $\Delta C_\pm = 10^{-7}$ M. This procedure is then repeated with an anchored chain, etc. After computing the convergent values of $C_\pm$ and V at each time unit of the Langevin simulation, the ionic current at this time t is given by

$$I(t) = A(J_+ + J_-) \tag{2.9}$$

with

$$J_\pm(\mathbf{r},t) = -D_\pm\left(\nabla C_\pm(\mathbf{r},t) + \frac{Z_\pm C_\pm}{k_B T}\nabla V(\mathbf{r},t)\right) \tag{2.10}$$

In evaluating the ionic current, we have taken $J_\pm$ at $X = 0$ and the cross-sectional area A at this exit point is 441 Å^2.

The simulation efforts are divided into two parts. The first part is the investigation of a polymer chain tethered to the α-hemolysin. At the beginning of the simulation, the tethered PEG is equilibrated for typically 10^5 time steps. After equilibration, data on the positions of the polymer beads are gathered every 1000 time steps during the next million steps. Simulations are carried out for various anchoring positions, different values of temperature T, and polymer length N. Reduced temperature units are used throughout the simulations. Since the temperature is coupled with potential energy, changing temperature is equivalent to tuning solvent quality. Thus, the Lennard-Jones interaction parameters are fixed. During the course of every simulation, the instantaneous ionic current is calculated from the PNP equations. For the purpose of comparisons, free polymer chains in the absence of the pore and membrane are also simulated. The second part of the simulations focuses on the capture of streptavidin. After the equilibration of the biotinylated PEG, the center of mass of streptavidin is placed about 15 units away from the pore opening in the *cis* chamber. An applied electric field is turned on to drive the streptavidin toward the pore. The binding between the biotinylated PEG and streptavidin and the ionic current are monitored simultaneously. The simulations of streptavidin capture in the *trans* chamber are performed in a similar manner.

3. Results and Discussion

3.1. Polymer Tethered to the Protein Pore. We begin our investigation by examining the conformations of an isolated free polymer chain, without any confinement, before addressing the influence of αHL. For the value of $\sigma = 0.4$, the mean square radius of gyration $\langle R_g^2 \rangle$ is plotted in Figure 2 against the reduced temperature $T_r = k_B T/\epsilon_{LJ}$ for different chain lengths. This figure exhibits the coil−globule transition. At higher temperatures, the chain is swollen due to excluded volume interactions and obeys

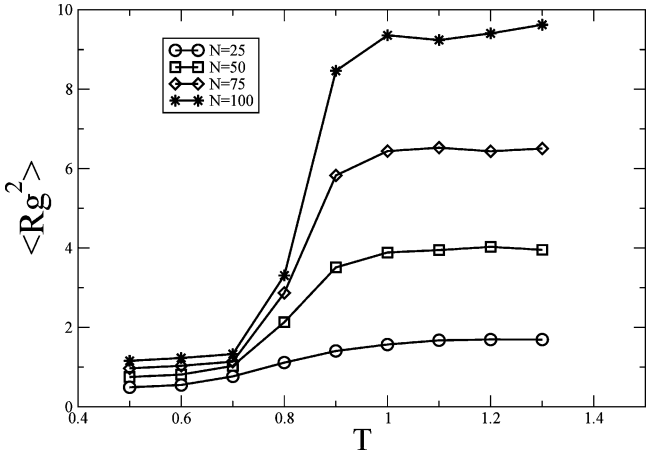

Figure 2. The mean square radius of gyration is plotted as a function of reduced temperature for $N = 25$, 50, 75, and 100.

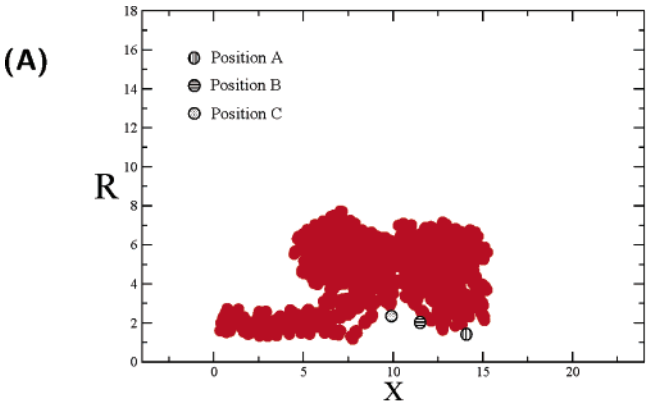

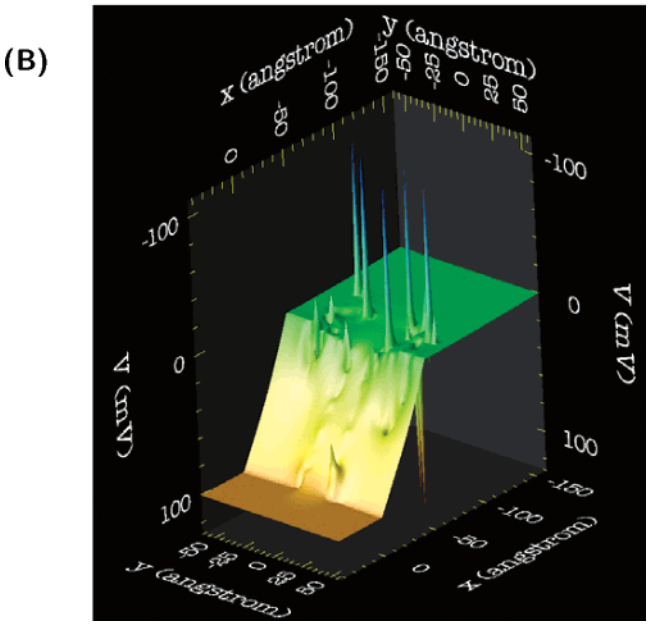

Figure 3. (A) Three anchoring positions of the polymer in the simulation are shown in cylindrical coordinates. (B) Fixed at $Z = 0$, the electrostatic potential on the $X-Y$ plane around the pore is plotted. The applied potential difference is 100 mV.

(36) Selberherr, S. *Analysis and Simulation of Semiconductor Device*; Sringer-Verlag: New York, 1984.
(37) Hollerbach, U.; Chen, D.-P.; Eisenberg, R. S. *J. Sci. Comput.* **2002**, *16*, 373.

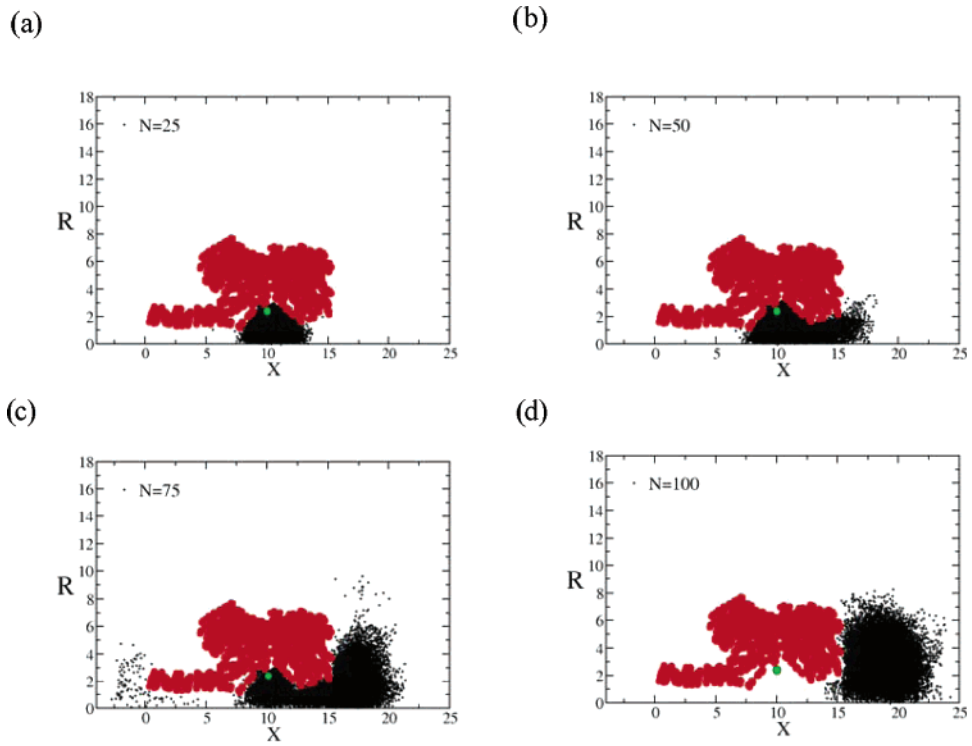

Figure 4. For $T = 0.9$ and $N = 25$, 50, 75, and 100, the scatter plots of the polymer end are shown in cylindrical coordinates. Each point in a plot represents one record during the simulation.

the excluded volume statistics of $R_g \sim N^{0.6}$. At lower temperatures, the chain is a globule with $R_g \sim N^{0.33}$. In terms of the reduced temperature, the coil−globule transition temperature for the model polymer chain is around 0.85. For $T_r \geq 0.9$, the model chain obeys the excluded volume statistics, that is, the chain is in a good solution. Under these conditions, the chain is considerably swollen in contrast to compact conformations.[39] It must be pointed out that aqueous solutions of PEG have an upper and lower critical solution temperatures of −9 and +103 °C, respectively, extrapolated from experimental data.[40,41] Since, at room temperature, PEG in water is known to obey the excluded volume statistics,[40,41] reduced temperatures in our simulations with values of 0.9 and above correspond to the experimental conditions of stochastic sensing by the PEG−αHL pore.

We proceed to examine the chain end distribution of a polymer tethered to the protein pore. The three different anchoring positions *A*, *B*, and *C* corresponding to the residues Lys-8, Tyr-101, and Ser-106 of α-hemolysin, respectively, are shown in Figure 3A. Here, the pore is represented using the cylindrical symmetry with *X* along the central axis of the pore and *R* being the radial distance away from the central axis. First, the steady-state electrostatic potential across α-HL is computed using the PNP scheme, in the absence of the tether. A representative result is given in Figure 3B for 0.3 M KCl solution under an applied potential difference of 100 mV. In this figure, the axis *X* into the plane is the distance along the channel. Here $X = -100$ and 0 Å correspond, respectively, to the mouth of the vestibule and the *trans*-edge of the β-barrel. The potential is 0 mV at $X = -150$ Å and 100 mV at $X = 50$ Å. The ordinate is the electrostatic potential, and the abscissa is the *Y* axis, which is radially symmetric. The potential gradient is essentially zero in the donor and recipient compartments. The sharpest gradient is at the entrance to the β-barrel. Inside the vestibule, the potential gradient is weak. The delta function peaks inside the vestibule correspond to the presence of charged residues inside the lumen. The peaks with positive (negative) values represent positive (negative) charges. It is this electrical potential gradient that is responsible for the ionic current. With the tethered polymer, the instantaneous potential depends on the conformation of the polymer.

For $T_r = 0.9$ and $N = 25$, 50, 75, and 100, the scatter plots of the polymer end position are plotted in Figure 4 for the anchoring position *C*. Each dot represents a realization of the chain end at the location of the dot. The data were obtained by monitoring the chain conformations over times longer than the chain correlation time ($\sim N^2$). For small chain length ($N = 25$), the end of the tethered polymer stays within the vestibule. When a chain of *N* segments is confined in a cavity of volume v under good solution conditions, the free energy due to the excluded volume interaction is proportional[19,39] to N^2/v. The pressure due to this interaction is proportional to N^2. As the length increases, the pressure from both the excluded volume interaction between monomers and the entropic force of polymer confinement attempts to expel the chain out of the vestibule. As seen in the case of $N = 50$, the polymer begins to explore the *cis* chamber, outside the αHL vestibule. Since the β-barrel is narrow and entropically unfavorable for the polymer to visit, the polymer end avoids entering the β-barrel. When the polymer length increases to $N = 75$, the internal pressure is built up to an unsustainable level for polymer confinement inside the vestibule.

(38) Schuss, Z.; Nadler, B.; Eisenberg, R. S. *Phys. Rev. E* **2001**, *64*, 0361161.
(39) De Gennes, P. G. *Scaling Concepts in Polymer Physics*; Cornell University Press: Ithaca, NY, 1979.
(40) Boucher, E. A.; Hines, P. M. *J. Polym. Sci., Polym. Phys. Ed.* **1976**, *14*, 2241.
(41) Molyneux, P. *Water-Soluble Synthetic Polymers: Properties and Behavior*; CRC Press: Boca Raton, FL, 1983; Vol. 1.

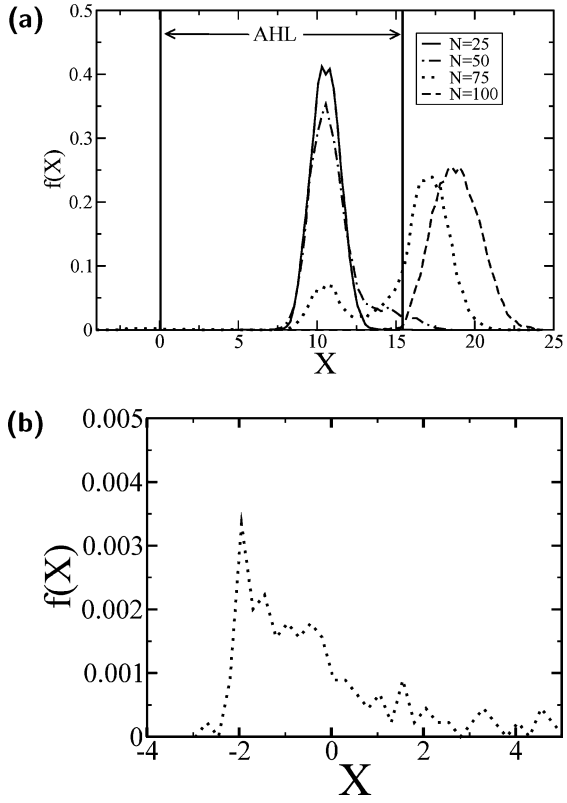

Figure 5. (a) Probability distribution functions for different polymer lengths are plotted for $T = 0.9$ and anchoring position C. (b) For $N = 75$, the polymer end can completely thread through the β-barrel.

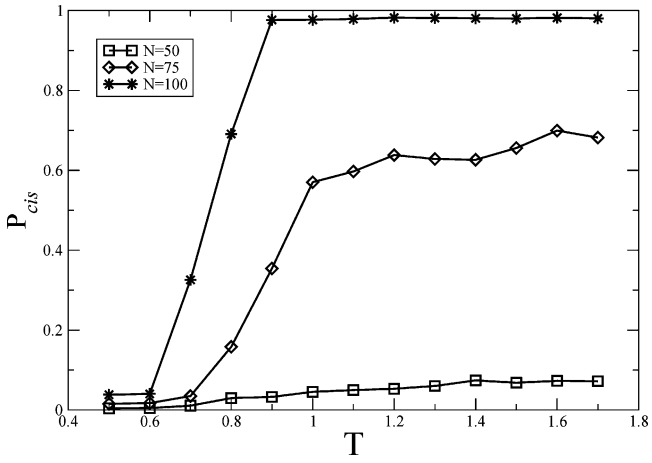

Figure 6. The temperature dependence of the probability of finding the polymer end outside the vestibule for anchoring position C.

Being expelled and tethered at the same time, the polymer attempts to explore both the *cis* and *trans* chambers as shown in Figure 4c. For $N = 100$, the pressure completely pushes the free end of the polymer out of the vestibule and into the *cis* chamber. To facilitate an easier visualization of data, the probability distribution function $f(X)$ of finding the free polymer end along the central axis of the protein pore is plotted in Figure 5. X is the distance along the central axis of the pore. The pore extends from 0 (interface between the membrane and the *trans* chamber) to 15 (mouth of the vestibule toward the *cis* chamber). For $N = 25$, the chain end is around $X = 10$ at the center of the vestibule. As N increases, the probability to find the end in the *cis* chamber increases progressively, and for $N = 100$, the chain end is essentially outside the vestibule. The probability of finding

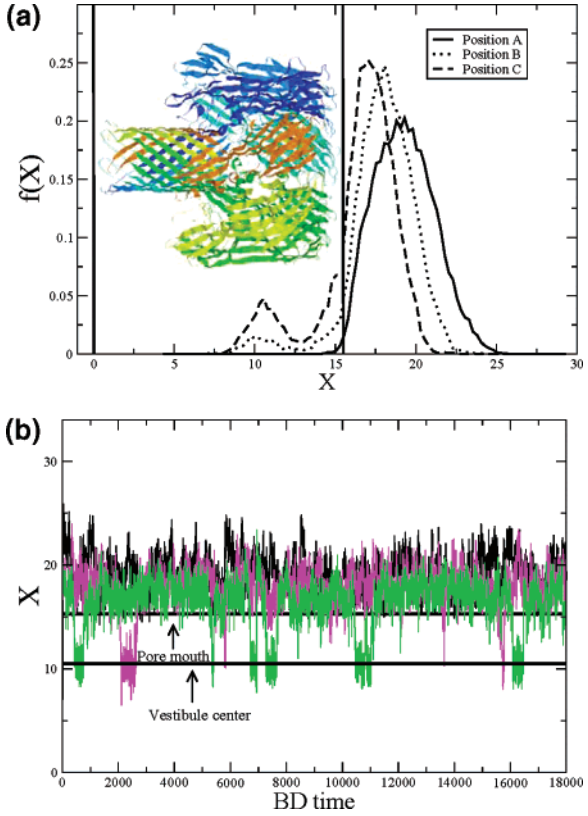

Figure 7. (a) Probability distribution functions with different anchoring positions of the polymer for $N = 75$ and $T = 1.2$ are plotted. A cartoon of the α-hemolysin pore is shown to mark the pore position in the simulations. (b) Position of the free polymer end along the central axis of the pore as a function of time is plotted. The locations of the pore mouth and vestibule center are shown.

the chain end in the *trans* chamber ($X < 0$) is given in Figure 5b. Here, only the chain of intermediate length ($N = 75$) is able to explore the *trans* side. For other chain lengths ($N = 25$, 50, 100), $f(X)$ is essentially zero. The nonmonotonic dependence of $f(X < 0)$ on N arises mainly due to the pressure generated inside the vestibule. For short chains, the pressure due to excluded volume interactions is not enough to thread the polymer into the β-barrel. However, for long chains, the pressure is too high to push the chain into a thermodynamically more stable situation of exploring the large *cis* chamber instead of the confining β-barrel. For intermediate chain lengths, the chain is long enough to thread through the β-barrel, and the pressure is not too high to completely push the chain out of the vestibule.

We then proceed to examine the effect of temperature on the chain end distribution of the polymer tethered at location *C*. The probability of finding the free polymer end being outside the vestibule P_{cis} is plotted in Figure 6 as a function of temperature. P_{cis} is calculated by integrating the probability distribution function outside the *cis* opening of the α-hemolysin. As shown in Figure 2, the polymer chain undergoes coil−globule transition as the temperature is reduced. The tendency of the chain to be more compact at lower temperatures reduces the probability of the free end outside the vestibule. This is borne out in Figure 6. The sharpness of the change in P_{cis} with temperature increases with chain length, reflecting the sharpness of the inherent coil−globule transition with respect to the chain length.

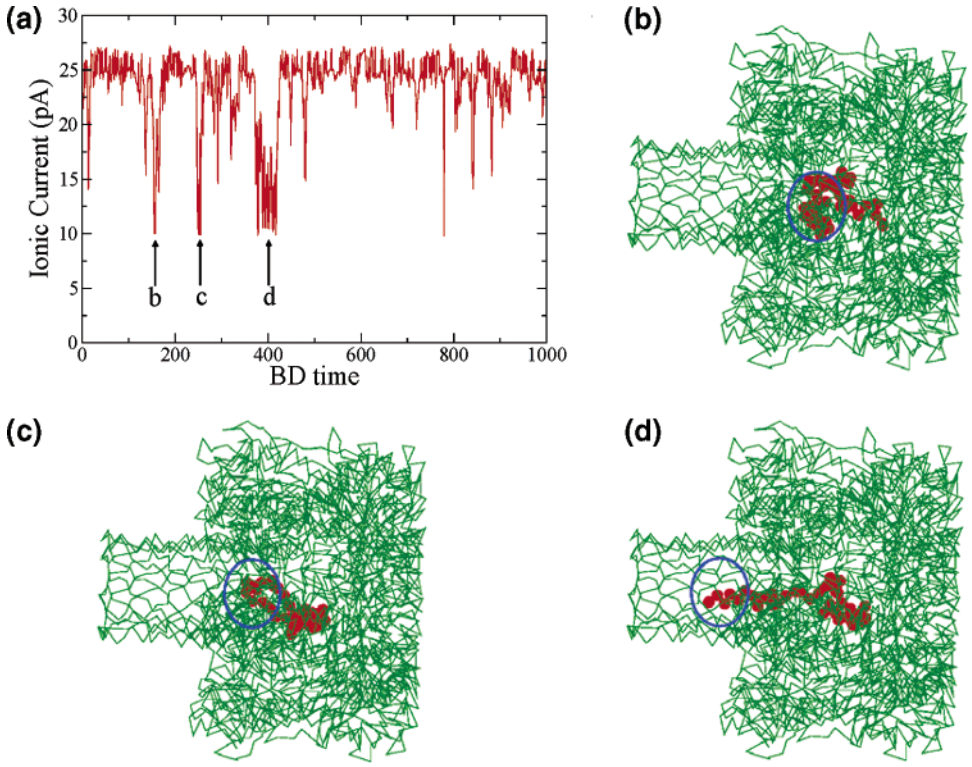

Figure 8. (a) Plot of calculated ionic current as a function of time. (b and c) Snapshots taken from the simulation indicate the physical origin of the negative spikes. (d) Snapshot with threading.

The location of the anchoring position of the polymer inside the vestibule plays a crucial role in determining $f(X)$, as demonstrated in Figure 7a, for $T_r = 1.2$ and $N = 75$. When one end of the polymer is tethered near the mouth of the pore (position A), the free end resides mostly in the *cis* chamber. Tethering the polymer inside of the vestibule at positions B and C, the polymer end is able to fold back and enter the vestibule. This shows that changing the anchoring position of the polymer is an effective way to control the location of the free polymer end, as can readily be envisaged from geometrical considerations. For $T = 1.2$ and $N = 75$, the position of the free polymer end along the central axis of the pore as a function of time is plotted in Figure 7b. When the polymer is tethered at position A, the end stays fully outside the vestibule. Anchoring at positions B and C, the location of the end fluctuates between being inside the vestibule and outside it. The frequency of residence of the chain end inside the vestibule increases with the depth of the anchoring position toward the β-barrel.

We now proceed to calculate the ionic current. To interpret the signals received by the sensor, the first step is to understand the behavior of the ionic current through the α-hemolysin pore. For the αHL geometry, our PNP calculations give the open pore current to be 25 pA for 0.3 M KCl (used in experiments). This is in agreement with experimental values. It is remarkable that mean field theories, such as the PNP formalism, are applicable even for nanoscale pores such as αHL. This success is probably due to the short Debye length in the system, as discussed in refs 36 and 38. Next, we repeat the calculation of the ionic current as the tether anchored at a prescribed location fluctuates. Experimentally, current fluctuations with short-lived high amplitude spikes are observed when a PEG molecule is anchored within the cavity of α-hemolysin. Howorka and co-workers[5] suggested that the short-lived, high amplitude, negative current spikes may represent the partial looping of the PEG chain into the transmembrane barrel or into the *cis* opening. It was also suggested that the spikes are caused by the excursions of the polymer end toward the *trans* entrance into the transmembrane β-barrel.[6] All of these conjectures can be tested by monitoring chain conformations in our simulations.

In the following illustrative plot of ionic current versus time, given in Figure 8, $N = 40$, $T_r = 1.0$, and the anchoring location is at the position C. As seen in experiments, simulations exhibit many negative short-lived spikes in the ionic current trace. The value of the ionic current at the peaks of the negative fluctuations is about 10 pA, in good agreement with the experimental results. A closer examination of the current trace reveals that the appearance of the spikes coincides with the polymer segments obstructing the entry of the β-barrel as indicted in Figure 8b,c. The polymer end does not necessarily have to thread into the β-barrel to cause the negative spikes. In the case of polymer end threading, as shown in Figure 8d, the spikes are almost indistinguishable from the case of polymer segments obstructing the β-barrel. What really causes the negative spikes in the ionic current is the physical blockade of area at the mouth of the β-barrel by the tether so that only a lesser number of ions can be transported. This physical blockade can be caused either by threading into the β-barrel or by obstructing the entry of small ions. In our simulations, we see the latter. One of the major conclusions that can be reached from our simulations is that the magnitude of the ionic current through the αHL pore at any given time is simply dependent on the surface area available at the mouth of the β-barrel for small electrolyte ions to be transported. This simple rule can be taken advantage of in designing stochastic sensors.

3.2. Analyte Detection by the Modified Pore. We now study the capture of protein analytes by the modified pore. All of the

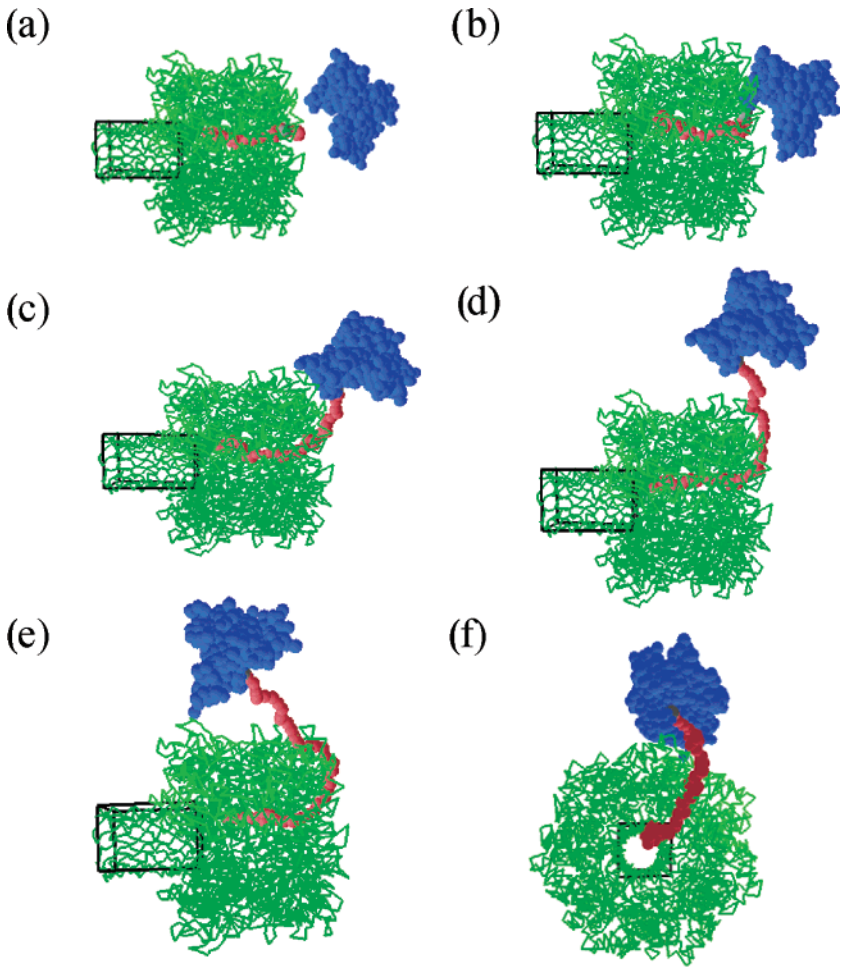

Figure 9. (a−f) Correspond to the positions of the analyte and the tethered polymer during a capture event. The simulation time is (a) 141, (b) 301, (c) 361, (d) 601, (e) 651, and (f) 671 (side view).

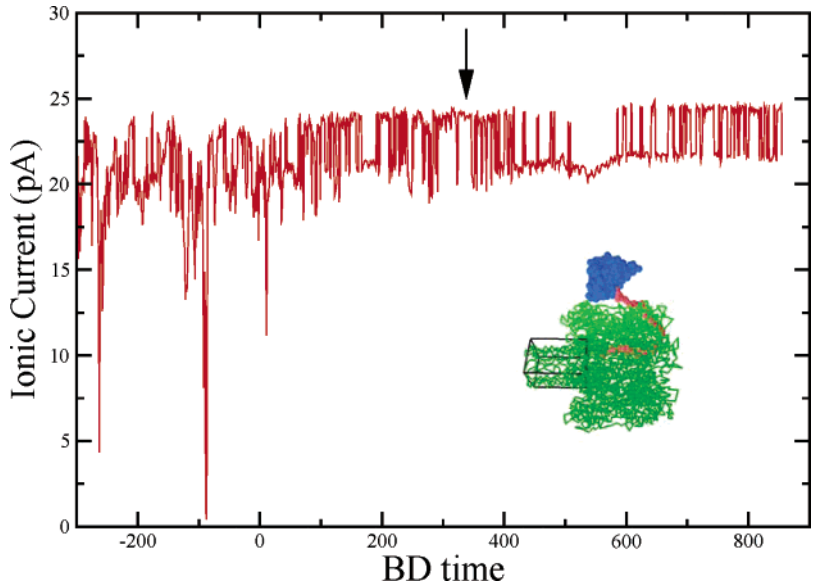

Figure 10. The ionic current trace of a capture event in the *cis* chamber is plotted as a function of simulation time. The black arrow indicates the time of protein capture.

following results correspond to the situation of the polymer being anchored at the position C. We first present the results for the capture of the wild-type streptavidin proteins in the *cis* chamber. To provide insight into the capture event, snapshots of a typical simulation are shown in Figure 9a−f. The length of the polymer is $N = 40$. Initially, the protein analyte is aiming at the opening of the modified pore on the *cis* side. Due to the net negative surface charges, the protein analyte moves toward the pore. Since streptavidin is too large to fit into the pore, it collides with the pore. The polymer chain acts as an entropic

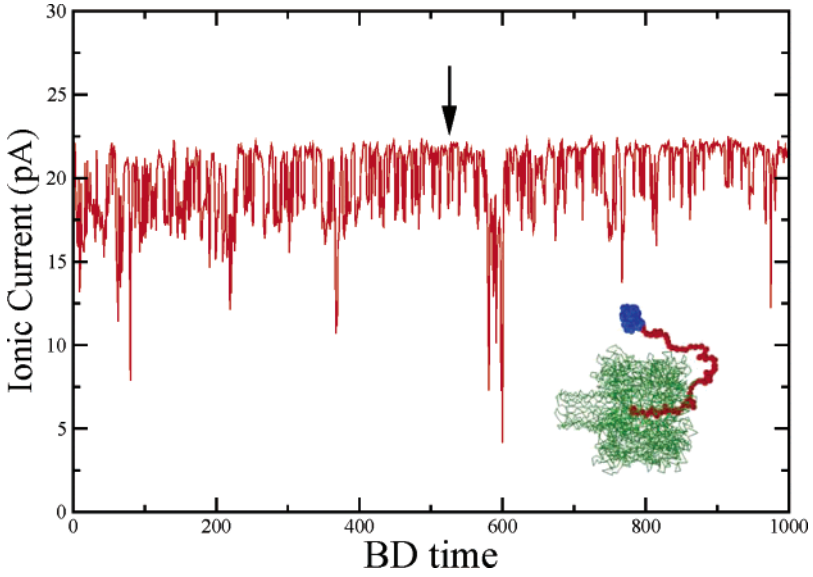

Figure 11. For a longer polymer, the ionic current trace of a capture event in the *cis* chamber is plotted. Due to the incommensurate chain length, the ionic current does not show silencing.

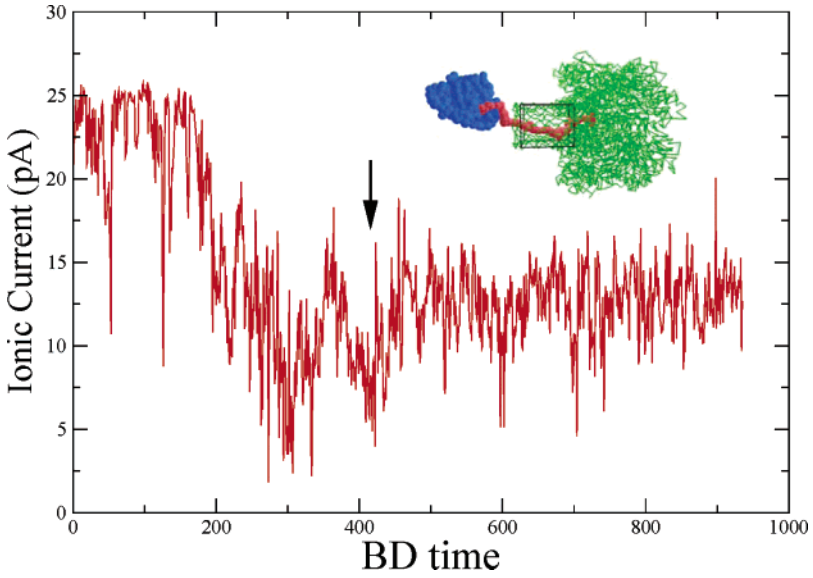

Figure 12. The ionic current trace of a capture event in the *trans* chamber.

spring and pushes the streptavidin to the side by chain fluctuations, as shown in Figure 9b−d. During the collision, the streptavidin is captured by the biotinylated PEG. As the streptavidin rolls off to the side of the pore, the anchored PEG polymer is pulled out of the vestibule. When the streptavidin hits the membrane surface, the PEG is completely taut, as shown in Figure 9e,f. For this particular capture event, the ionic current is shown in Figure 10, and indeed, silencing of the ionic current is observed. As discussed in the last section, the negative spikes are caused by the fluctuating polymer obstructing the mouth of the β-barrel. By the taut, the polymer chain is stretched, and its fluctuations inside the vestibule are substantially reduced. As a result, the ionic current becomes silent. If the contour length of the polymer is too long, the streptavidin is stopped by the membrane before the polymer gets fully taut. Now, the polymer chain is expected to contain some residual fluctuations, although the complexation has already occurred. This is illustrated in Figure 11 for a longer chain ($N = 75$). The values of all other parameters are the same in both Figures 10 and 11. For $N = 75$, the contour length is more than the length required for just the full taut. Therefore, as seen in Figure 11, the ionic current shows persistent fluctuations (without any silencing), even though the binding has already occurred (as indicated by the arrow in the figure). Therefore, we conclude that the length of the tether and its anchoring location have to be just right for the strategy of fishing-line to work in stochastic sensing. More significantly, the process of stochastic sensing occurs via current modulation.

For the case of pore-silencing, we have repeated the simulation by weakening the binding affinity between streptavidin and biotin, to study the differences between the mutant and wild-type streptavidin in experiments. As already mentioned in section 2, ϵ_{LJ} for the mutant streptavidin−biotin is taken to be 16 instead of 30 for the corresponding wild-type streptavidin. The results for $N = 40$, $T_r = 1.0$, and 0.3 M KCl are shown in Figure 12. Now the complexation between the biotin and streptavidin is reversible. When they are bound, the pore is silent. When they dissociate, the pore current shows fluctuations

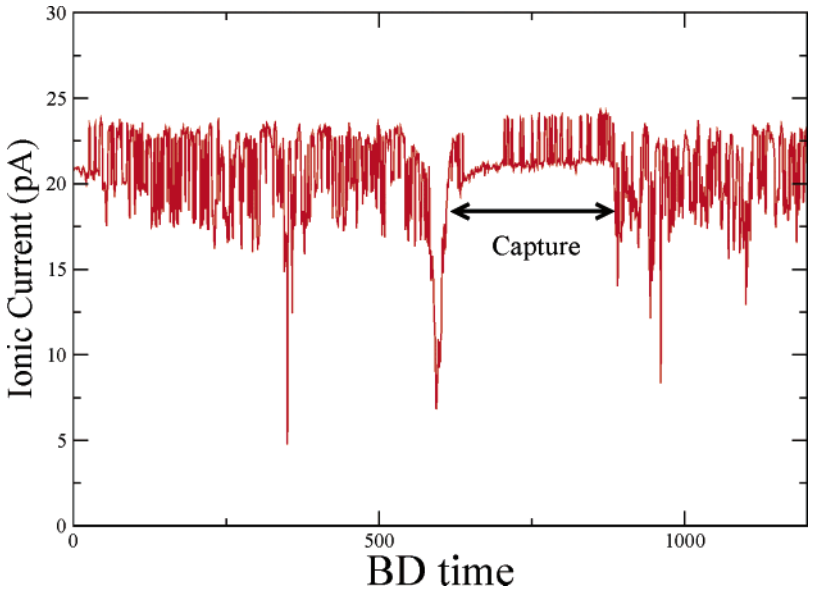

Figure 13. The ionic current trace of a reversible capture event in the *cis* chamber.

representing the conformational fluctuations of the tether. These simulation results are in full accord with the original interpretation of the experimental data.

Next, we have simulated the capture of the wild-type streptavidin dispersed in the *trans* chamber. The ionic current trace for $N = 40$, $T_r = 1.0$, and 0.3 M KCl is given in Figure 13. When the protein is complexed with the polymer end, the ionic current is permanently blocked. However, the onset of blockade of ionic current cannot be identified with the time of capture, which is indicated in Figure 13. The ionic current blockade begins as soon as the tether is able to thread through the β-barrel. It is also to be noted that the threaded tether inside the β-barrel supports some ionic current due to the diameter of the tether backbone being smaller than that of the pore. All of the simulation results are in agreement with all qualitative features of experimental data and provide molecular details of the observed phenomena. Although precise quantitative comparison is precluded due to the coarse-grained nature of the modeling scheme, the present technique provides a satisfactory and efficient method to understand the various mechanisms of stochastic sensing arising from polymer properties.

4. Conclusions

Using the Langevin dynamics and Poisson−Nernst−Planck calculations, we have investigated the effects of length and anchoring location of the PEG tether (inside αHL) on the distribution function of the free end of the polymer. As the tether length increases, the entropic pressure to confine the tether inside the vestibule of αHL builds up, which leads to the preferential expulsion of the free end of the tether into the *cis* chamber. Due to the same origin, the small probability of finding the tether end in the *trans* chamber depends on tether length nonmonotonically. As expected, the probability of finding the free end of the tether in the *cis* chamber is enhanced if the anchoring position of the other end is closer to the mouth of the vestibule. The effect of the incipient coil−globule transition on the distribution function has also been monitored in terms of an effective temperature reflecting solvent quality. Lowering the temperature leads to more compact conformations of the tether, which in turn leads to lower probability of the free end being outside the vestibule.

The PNP calculations show that the short-lived high amplitude spikes in the ionic current traces are due to the obstruction of the β-barrel by conformational fluctuations of the tether. These strong spikes are absent and the pore becomes silent if the conformational fluctuations of the tether are suppressed. This is seen in our simulations to arise from the tautening of the tether after complexation between the free end and the analyte in the *cis* chamber. If the tether threads through the β-barrel, the ionic current is blocked substantially, and the threading is a necessary step for capture of the analyte in the *trans* chamber. Vivid details from our simulations show that signals in the ionic current traces can be out of synchronization with the capture events. With the expected future applications of stochastic sensing techniques, our method of combining Langevin dynamics simulations and PNP equations may provide a novel and powerful theoretical approach in the designing process.

Acknowledgment. It is a pleasure to thank Professor Hagan Bayley for many stimulating discussions. Acknowledgment is made to NIH Grant No. 1R01HG002776-01, NSF Grant No. DMR-0209256, and to the donors of The American Chemical Society Petroleum Research Fund for support of this research.

JA055695O